J Fluoresc (2009) 19:203–209
DOI 10.1007/s10895-008-0403-5

ORIGINAL PAPER

Modeling the Relative Fluorescence Intensity Ratio of Eu(III) Complex in Different Solvents Based on QSPR Method

Jie Xu · Qi Xiong · Biao Chen · Luoxin Wang · Li Liu · Weilin Xu

Received: 4 June 2008 / Accepted: 14 July 2008 / Published online: 30 July 2008

Abstract The quantitative structure-property relationship approach was performed to study the relative fluorescence intensity ratio (R) of Eu(DBM)$_3$Phen (DBM—dibenzoylmethane, Phen—1,10-phenanthroline) in 34 different solvents. The multilinear regression analysis and artificial neural networks were employed to develop linear and nonlinear models, respectively. The proposed linear model contains six descriptors, with the squared correlation coefficient r^2=0.955 and the standard error of estimation s=1.02. Better predictive results were obtained from the nonlinear model, with r^2=0.987 and s=0.51. The descriptors involved in the models were discussed in detail too.

Keywords QSPR · Eu(DBM)$_3$Phen · Relative fluorescence intensity ratio · Multilinear regression analysis · Artificial neural networks

J. Xu (✉) · Q. Xiong · L. Wang · W. Xu
Key Laboratory of Green Processing and Functional Textiles of New Textile Materials, Ministry of Education, Wuhan University of Science and Engineering, Wuhan 430073, China
e-mail: xujie0@ustc.edu

B. Chen
Department of History of Science and Technology and Archaeometry, University of Science and Technology of China, Hefei 230026, China

L. Liu
College of Electronics and Information Engineering, Wuhan University of Science and Engineering, Wuhan 430073, China

Introduction

Lanthanide complexes have been well known to give bright emission under ultraviolet irradiation because of the effective energy transfer from ligands to central ions (an antenna effect) and have been found in some applications such as in optical devices, luminescence probes in biomedical assays, fluorescent and electroluminescent lighting devices [1–5]. The emission properties of this family of complexes are notable and cover an exceptionally wide spectral range: near-infrared (Nd^{3+}, Er^{3+}, Pr^{3+}), red (Eu^{3+}, Pr^{3+}, Sm^{3+}), green (Er^{3+}, Tb^{3+}), and blue (Tm^{3+}, Ce^{3+}) [6]. In particular, europium and terbium β-diketonate complexes have been extensively studied [7–11] due to their high fluorescence efficiency. Lanthanide complexes are widely used as solutes or dopants in various host compounds [3, 5, 12–14]. However, the local structure and composition surrounding lanthanide complexes strongly influence the fluorescent properties, such as relative intensity, quantum yield and luminescent life decay. Thus, it is of great importance to investigate the relationships between the fluorescent properties of lanthanide complexes and the molecular structures of host compounds.

The quantitative structure-property relationship (QSPR) has become an important area of research in cheminformatics. The QSPR approach is based on the assumption that the variation of the behavior of the compounds, as expressed by any measured physicochemical properties, can be correlated with changes in molecular features of the compounds termed descriptors [15, 16]. The advantage of this approach lies in the fact that it requires only the knowledge of the chemical structure and is not dependent on any experimental properties. Once a correlation is established, it can be applicable for the prediction of the property of new compounds that have not been synthesized

or found. Thus the QSPR approach can expedite the process of development of new molecules and materials with desired properties. Furthermore, some insights into the chemical, physical and physicochemical phenomena related to the property under investigation could be obtained by interpreting the descriptors in the correlation.

Using the QSPR approach, many attempts have successfully been made to study the spectral properties of various systems [16–20]. Shi et al. [18] performed the QSPR study for the modeling of fluorescence wavelengths of fluorescence probes using heuristic method and radial basis function neural networks. Nantasenamat et al. [19] investigated the prediction of the excitation and emission maxima of green fluorescent protein chromophores using an artificial neural network. Li et al. [20] developed successful linear and nonlinear QSPR methods to predict the fluorescence excitation wavelengths of boronic acid-based fluorescent biosensors. But to our knowledge, there are no examples of QSPR studies on fluorescent properties of lanthanide complexes in different solvents.

The goal of the present work is (1) to model the relative fluorescence intensity ratio of $Eu(DBM)_3Phen$ in different solvents, (2) to discover the main structural factors of solvents that affect this property significantly.

Materials and methods

$Eu(DBM)_3Phen$ was synthesized according to the literature [21] and its molecular structure is shown in Fig. 1. The IR spectrum of $Eu(DBM)_3Phen$ was measured on a Nicolet170 SX fourier transform infrared spectrophotometer using the KBr pellet technique. Absorptions corresponding to functional groups can be found in the spectrum, such as C=O group at 1,595.1 cm^{-1}, Phen group at 1,549.9 cm^{-1}, C=C group in the enol structure at 1,517.9 cm^{-1} and Eu–O group at 511.6 cm^{-1}. The elemental analysis was performed using an Elementar Vario EL-III elemental analyzer. $EuC_{57}H_{44}O_6N_2$ (1,004.93): calcd. C 68.12, H 4.41, N 2.79; found C 68.14, H 4.07, N 2.78. Solutions of $Eu(DBM)_3Phen$ in 34 different solvents (0.005 mol/l) were prepared. The fluorescence emission spectra were recorded on a Shimadzu RF-5301PC (Japan) spectrofluorophotometer. The emission peaks centered at 591 and 613 nm can be assigned to $^5D_0 \rightarrow {}^7F_1$ and $^5D_0 \rightarrow {}^7F_2$, respectively. The $^5D_0 \rightarrow {}^7F_1$ transition is usually used as a reference, because it is allowed by magnetic dipole and its intensity is independent of the local environment. The $^5D_0 \rightarrow {}^7F_2$ transition is allowed by induced electric dipole mechanisms, and its intensity strongly depends on the chemical environment in which Eu^{3+} ions are located. Therefore, the variation of the relative intensity ratio (R) of the $^5D_0 \rightarrow {}^7F_2$ to $^5D_0 \rightarrow {}^7F_1$ transition is very sensitive to the structural change in the vicinity of Eu^{3+} ions, which can be commonly used to reflect the local structure and composition of Eu^{3+} ions [22, 23]. The R values derived from the fluorescence spectra were listed in Table 1.

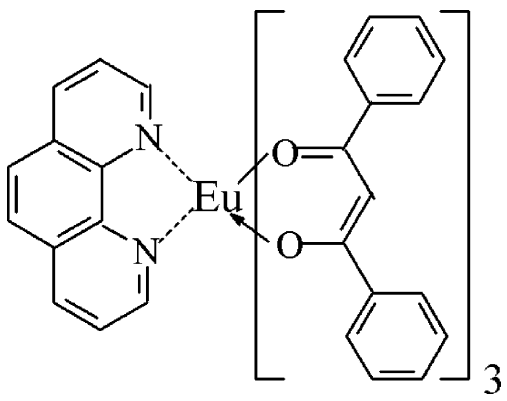

Fig. 1 The chemical structure of $Eu(DBM)_3Phen$

The structures of all solvent molecules were preoptimized using MM + molecular mechanics method (Polak–Ribiere algorithm) by means of the HYPERCHEM program [24]. The final geometries of the minimum energy conformation were obtained by the semi-empirical AM1 method using a gradient norm limit of 0.01 kcal·Å/mol. Then totally 1664 molecular descriptors for each solvent were computed on the minimal energy conformation through Dragon software [25]. These descriptors are classified as (a) 0D-constitutional (atom and group counts); (b) 1D-functional groups and atom centered fragments; (c) 2D-topological, BCUTs, walk and path counts, autocorrelations, connectivity indices, information indices, topological charge indices, and eigenvalue-based indices; and (d) 3D-Randic molecular profiles from the geometry matrix, geometrical, WHIM, and GETAWAY descriptors. In order to reduce redundant and non-useful information, constant or near constant values and descriptors found to be highly correlated pairwise (one of any two descriptors with a correlation greater than 0.99 [26]) were excluded in a pre-reduction step. Thus 678 molecular descriptors underwent subsequent descriptor selection.

Linear QSPR models were developed by applying stepwise multilinear regression analysis (MLRA) with Leave-One-Out (LOO) cross-validation to the data set. F-to-enter and F-to-remove were 4 and 3, respectively. The quality of the models was measured with the squared correlation coefficient r^2, the adjusted r^2, the cross-validated r^2, the F ratio values, the standard error of estimation s and the significance level value p. The adjusted r^2 is calculated using the following formula:

$$r^2_{adj} = 1 - \left[\left(\frac{N-1}{N-M-1}\right) r^2\right] \quad (1)$$

where N is the number of the samples and M is the number of descriptors involved in the correlation. The adjusted r^2 is

Table 1 Experimental and predicted R values of $Eu(DBM)_3Phen$ in different solvents

Solvents	R(expt.)	MLRA		ANNs	
		R(pred.)	ΔR [a]	R(pred.)	ΔR [a]
1,2-Divinylbenzene	9.57	9.34	0.23	9.61	−0.05
1,4-Butyrolactone	9.55	13.25	−3.71	10.73	−1.18
1,4-Dioxane	15.97	16.30	−0.34	15.84	0.13
4-Methyl-2-pyrrolidinone	16.74	16.02	0.72	16.68	0.05
Acetone	16.29	16.33	−0.05	15.85	0.44
Acetylacetone	11.78	12.55	−0.77	10.55	1.23
Acrylonitrile	15.62	16.39	−0.76	15.88	−0.25
Anisole	15.22	15.82	−0.60	15.75	−0.52
Bromobenzene	14.62	14.59	0.03	15.33	−0.71
Butyl acrylate	16.02	15.37	0.65	15.60	0.43
Butyl methacrylate	15.43	15.15	0.28	15.53	−0.11
Carbon tetrachloride	15.36	15.11	0.25	15.37	−0.01
Cyclopentanone	15.26	13.72	1.54	15.01	0.25
Dibutyl phthalate	13.46	13.00	0.46	13.44	0.02
Dichloromethane	15.47	15.99	−0.52	15.70	−0.23
Dimethyl phthalate	15.12	16.32	−1.20	15.13	−0.01
Dimethyl sulfoxide	16.33	15.94	0.39	15.67	0.65
Ethyl acrylate	16.46	15.35	1.11	15.64	0.82
Ethyl propionate	16.21	15.26	0.95	15.61	0.60
Isobutanoic acid	3.30	3.32	-0.03	3.28	0.01
Lactic acid	2.78	3.56	−0.79	2.78	−0.01
Methacrylic acid	3.80	3.68	0.12	2.82	0.97
Methyl methacrylate	15.70	15.44	0.26	15.65	0.05
m-Xylene	15.22	14.94	0.28	15.57	−0.35
N,*N*-Dimethylformamide	18.64	19.36	−0.72	18.67	−0.03
n-Octylic acid	2.90	2.21	0.69	2.91	−0.01
Phenyl methanol	14.75	15.35	−0.61	15.55	−0.81
p-Xylene	15.26	15.63	−0.36	15.70	−0.44
Styrene	14.94	15.12	−0.18	15.47	−0.52
Tetrahydrofuran	16.22	15.35	0.87	15.45	0.77
Toluene	15.73	15.61	0.12	15.70	0.03
Tributylphosphate	18.44	17.43	1.01	18.37	0.07
Trichloromethane	15.30	15.56	−0.26	15.53	−0.23
Vinyl acetate	15.59	14.68	0.91	15.52	0.07

[a] $\Delta R = R(\text{expt.}) - R(\text{pred.})$

a better measure of the proportion of variance in the data explained by the correlation than r^2 (especially for correlations developed using small datasets) because r^2 is somewhat sensitive to changes in N and M. The adjusted r^2 corrects for the artificiality introduced when M approaches N through the use of a penalty function which scales the result. A variance inflation factor (VIF) was calculated to test if multicollinearities existed among the descriptors, which is defined as

$$\text{VIF} = \frac{1}{1 - r_j^2} \tag{2}$$

where r_j^2 is the squared correlation coefficient between the jth coefficient regressed against all the other descriptors in the model. Models would not be accepted if they contain descriptors with VIFs above a value of five [27].

The proposed model was also checked for reliability and robustness by randomization tests: new models were recalculated for randomly reordered R values. The resulting models obtained on the data set with randomized R values should have significantly lower r^2 values than the proposed one because the relationship between the structure and property is broken. This is proof of the proposed model's validity as it can be reasonably excluded that the originally proposed model was obtained by chance correlation.

The nonlinear model was then developed by submitting the selected descriptors from MLRA to a three-layer, fully connected, feed-forward ANN. The number of input neurons was equal to that of the descriptors in the linear model. The number of hidden neurons was optimized by trial and error procedure on calculations of the training process. One output neuron was used to represent the experimental R. The network was trained using the quasi-Newton Broyden–Fletcher–Goldfarb–Shanno (BFGS) algorithm [28]. To avoid overtraining, one tenth data from the data set were randomly selected as separate validation set to monitor the training process; that is, during the training of the network the performance was monitored by predicting the values for the systems in the validation set. When the results for the validation set ceased to improve, the training was stopped.

Results and discussion

Stepwise MLRA with LOO cross-validation was used to select the descriptors for the best model and the number of

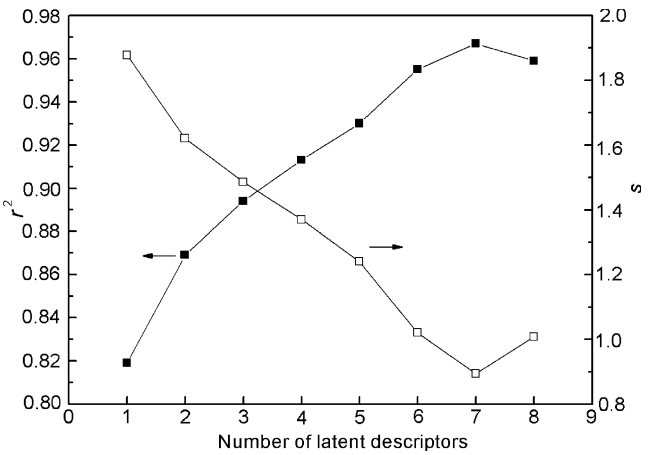

Fig. 2 r^2 and s vs. number of latent descriptors in the best MLRA models

Table 2 Characteristics of descriptors in the final MLRA model

Descriptor	Descriptor type	SE	*t*-value	*p*-level	VIF
Constant		0.314	52.233	0.000	
EEig10d	Edge adjacency indices	0.513	5.250	0.000	1.089
EEig11d	Edge adjacency indices	0.888	-5.320	0.000	1.477
JGI3	Topological charge indices	4.925	-4.031	0.000	1.182
RDF030p	RDF descriptors	0.242	-2.854	0.008	1.494
nRCOOH	Functional group counts	0.567	-22.160	0.000	1.091
N-072	Atom-centered fragments	0.776	3.823	0.001	1.088

descriptors in the final model was determined on the basis of the data set size and on the basis of the r^2, the adjusted r^2, the cross-validated r^2, the F, the s and the p. The r^2 and s results during the stepwise MLRA are shown in Fig. 2. It is clear that univariant correlations between R and the different descriptors have poor r^2 and s values. This indicates that R is not linearly correlated with any of the molecular descriptors. The equation with seven descriptors has the best r^2 and s values. However, from a statistical viewpoint the ratio of the number of the samples (N) and the number of descriptors in the correlation (M) should not be too low. Usually, it is recommended that N/M≥5. In the situation of this study, with 34 samples, six descriptors were selected. The final correlation equation is as the following:

$$R = 16.408 + 2.692 \times \mathrm{EEig10d} - 4.725 \times \mathrm{EEi11d} - 19.850 \times \mathrm{JG13} - 0.690 \times \mathrm{RDF030p} - 12.570 \times \mathrm{nRCOOH} + 2.966 \times N - 072$$
$$N = 34,\ r = 0.977,\ r^2 = 0.955,\ r_{\mathrm{CV}^2} = 0.944,\ r^2_{\mathrm{adj}} = 0.945,\ F = 95.13,\ s = 1.02 \quad (3)$$

Here *EEig10d* is the eigenvalue 10 from edge adjacency matrix weighted by dipole moments; *EEig11d* is the eigenvalue 11 from edge adjacency matrix weighted by dipole moments; *JGI3* is the mean topological charge index of order 3; *RDF030p* is the Radial Distribution Function—3.0/weighted by atomic polarizabilities; *nRCOOH* is the number of carboxylic acids (aliphatic); and *N-072* corresponds to the number of N atoms in RCO-N< or >N-X = X, respectively.

In general, the larger the magnitude of the F ratio, the better the model predicts the property values in the data set. The large F ratio of 95.13 indicates that Eq. 3 does an excellent job of predicting the R values. Eq. 3 has an adjusted r^2 value of 0.945, which indicates very good agreement between the correlation and the variation in the data. The cross-validated correlation coefficient $r^2_{\mathrm{CV}} = 0.955$ illustrates the stability of the model by focusing on the sensitivity of the model to the elimination of any single data point. The most predictive model with r^2=0.794 is obtained using randomization test, which proves the reality of Eq. 3. The characteristics and interactions of the six descriptors are given in Tables 2 and 3. The *t*-values indicate that all the descriptors are highly significant. The VIF values and the interactions suggest that these descriptors are weakly correlated with each other. Thus, the model can be regarded as an optimal regression equation. The predicted results for the R values from Eq. 3 are shown in Table 1 and Fig. 3.

According to the *t*-values (in Table 2), the most important descriptor in Eq. 3 is *nRCOOH*. The coefficient for this descriptor is negative, meaning that solvents with carboxylic acids would decrease the R values. The contribution of this descriptor to the R values is in agreement with the contribution that one could expect for the interactions between Eu^{3+} and carboxylic acids. The *EEig10d* and *EEig11d* descriptors encode information about

Table 3 Interactions of descriptors and R

	EEig10d	*EEig11d*	*JGI3*	*RDF030p*	*nRCOOH*	*N-072*	*R*
EEig10d	1						
EEig11d	0.274	1					
JGI3	−0.035	−0.056	1				
RDF030p	−0.176	−0.533	0.189	1			
nRCOOH	0.080	0.081	−0.272	−0.078	1		
N-072	0.055	0.055	0.215	−0.132	−0.091	1	
R	0.116	−0.184	0.093	−0.023	−0.905	0.228	1

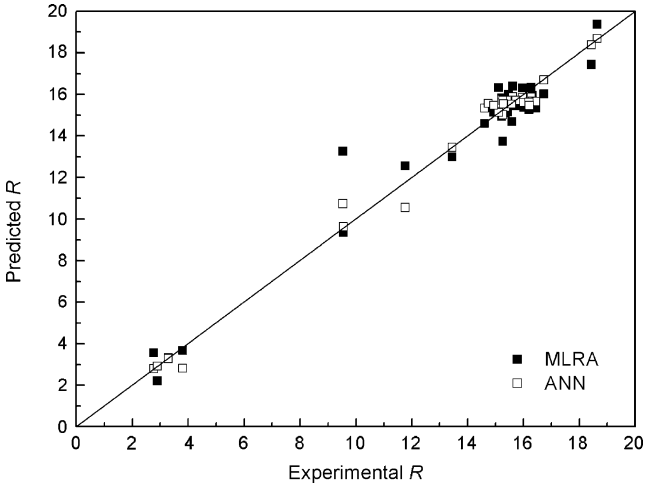

Fig. 3 Predicted vs. experimental *R* values for the MLRA and ANN models

the dipole moment of the molecule. The emergence of *EEig10d* and *EEig11d* in Eq. 3 indicate that the fluorescence and the site symmetry of Eu^{3+} are also influenced by the dipole moments of solvents. The importance of the transfers of intramolecular charge on the *R* values is apparent due to the presence of *JGI3* in Eq. 3. The positive sign of the *N-072* indicates that N atoms in RCO-N< or >N-X = X groups of solvent molecules would increase the *R* values. This effect is attributed to the coordination between Eu^{3+} and N atoms of solvents.

RDF030p is one of the RDF descriptors which have recently been proposed based on a radial distribution function. The RDF descriptors can be interpreted as the probability distribution of finding an atom in a spherical volume of radius *r*. The general form of the radial distribution function is represented by:

$$\mathrm{RDF}rw = f \cdot \sum_{i=1}^{nAT-1} \sum_{j=i+1}^{nAT} w_i \cdot w_j \cdot e^{-\beta(r-r_{ij})^2} \qquad (4)$$

where *f* is a scaling factor (assumed equal to one in the calculations), w_i and w_j are characteristic properties of the atoms *i* and *j* (including atomic number, masses, van der Waals volumes, Sanderson electronegativities, and polarizabilities), r_{ij} is the interatomic distance, and *nAT* is the number of atoms in the molecule [29]. *RDFrw* is generally calculated at a number of discrete points with defined intervals. Besides information about interatomic distances in the entire molecule, the *RDF030p* provides further information about atomic polarizabilities. The negative sign of the *RDF030p* indicates that Eu^{3+} in solvents with greater polarizabilites would have smaller *R* values and more symmetric location.

Recently, there is a growing interest in the use of ANNs for QSPR due to their inherent ability in modeling a nonlinear problem. The ANNs are especially useful when a rigid theoretical basis or mathematical relationship to describe a phenomenon to be modeled is not available. Among the neural network learning algorithms, the back-propagation (BP) method [30] is one of the most commonly used methods. The drawback of BP is that the training processes slowly, because the gradient-descent algorithm is usually used for minimizing the sum-of-squares error. In this study, the quasi-Newton BFGS algorithm was used. The advantages of using the BFGS algorithm are that specifying rate or momentum is not necessary and training processes are much more rapid [31].

The descriptors from the best MLRA model were used as inputs to the network. The number of hidden neurons is an important parameter influencing the performances of the ANNs. The usual rule of thumb is that the weights and biases should be less than the samples so that the model achieved by the network is stationary [32]. Thus, a 6–3–1 network architecture is obtained after trial and error procedure. The predicted results from the ANN model were given in Table 1 and Fig. 3 (r^2=0.987 and *s*=0.51). LOO cross-validation has also been carried out and R^2_{CV} of 0.985 is obtained, which indicates that there seems no chance correlation to happen. The distributions of the absolute errors (AEs) calculated with the MLRA and ANN models for the data set were shown in Fig. 4. With the MLRA model, the maximum AE is 3.71, the mean AE is 0.64, and only 6 samples have AEs less than 0.20; while with the ANN model, the maximum AE is 1.23, the mean AE is 0.35, and 15 samples have AEs less than 0.20. Evidently, these results show considerable modification in comparison to the MLRA model, which confirms the nonlinear relationship between structural information and *R* values.

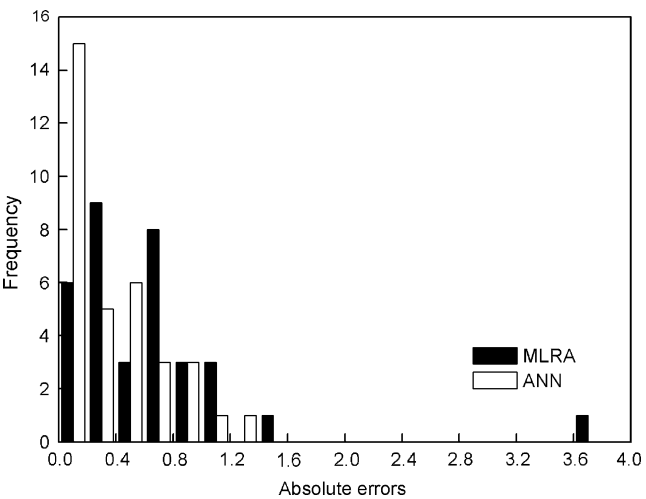

Fig. 4 Distributions of absolute errors calculated with the MLRA and ANN models

Conclusion

In this paper, both linear and nonlinear QSPR models are presented for the prediction of relative fluorescence intensity ratio of $Eu(DBM)_3Phen$ in different solvents. The predicted results are in good agreement with experimental values. The nonlinear model appears to be more reliable than the linear model. Therefore, this QSPR approach should be used as a promising tool for the prediction of relative fluorescence intensity ratio. The corresponding descriptors can also contribute to the fluorescent profiling of Eu $(DBM)_3Phen$ in different solvents.

Acknowledgements This work was supported by the Foundation of Wuhan University of Science & Engineering (No. 20073208), the Natural Science Foundation of Hubei Province (No. 2007ABA075), and the Key Project of Science and Technology Research of Ministry of Education (No. 208089). The authors gratefully wish to express their thanks to the reviewers for critically reviewing the manuscript and making important suggestions.

References

1. de Sá GF, Malta OL, de Mello Donegá C, Simas AM, Longo RL, Santa-Cruz PA et al (2000) Spectroscopic properties and design of highly luminescent lanthanide coordination complexes. Coord Chem Rev 196:165–195, doi:10.1016/S0010-8545(99)00054-5
2. Kido J, Okamoto Y (2002) Organo lanthanide metal complexes for electroluminescent materials. Chem Rev 102:2357–2368, doi:10.1021/cr010448y
3. Liang H, Zhang Q, Zheng Z, Ming H, Li Z, Xu J et al (2004) Optical amplification of $Eu(DBM)_3Phen$-doped polymer optical fiber. Opt Lett 29:477–479, doi:10.1364/OL.29.000477
4. Tremblay MS, Halim M, Sames D (2007) Cocktails of Tb^{3+} and Eu^{3+} complexes: A general platform for the design of ratiometric optical probes. J Am Chem Soc 129:7570–7577
5. Kuriki K, Koike Y (2002) Plastic optical fiber lasers and amplifiers containing lanthanide complexes. Chem Rev 102:2347–2356, doi:10.1021/cr010309g
6. Maas H, Currao A, Calzaferri G (2002) Encapsulated lanthanides as luminescent materials. Angew. Chem Int Ed 41:2495–2497, doi:10.1002/1521-3773(20020715)41:14<2495::AID-ANIE2495>3.0.CO;2-G
7. Su C, Kang B, Liu H, Wang Q, Chen Z, Lu Z et al (1999) Luminescent lanthanide complexes with encapsulating polybenzimidazole tripodal ligands. Inorg Chem 38:1374–1375, doi:10.1021/ic980899+
8. Alpha B, Lehn JM, Mathis G (1987) Energy transfer luminescence of europium(III) and terbium(III) cryptates of macrobicyclic polypyridine ligands. Angew Chem Int Ed Engl 26:266–268, doi:10.1002/anie.198702661
9. Wang L, Wang W, Zhang W, Kang E, Huang W (2000) Synthesis and luminescence properties of novel Eu-containing copolymers consisting of Eu(III)-acrylate-β-diketonate complex monomers and methyl methacrylate. Chem Mater 12:2212–2218, doi:10.1021/cm000158i
10. Bassett AP, Magennis SW, Glover PB, Lewis DJ, Spencer N, Parsons S et al (2004) Highly luminescent, triple- and quadruple-stranded, dinuclear Eu, Nd, and Sm(III) lanthanide complexes based on bis-diketonate ligands. J Am Chem Soc 126:9413–9424, doi:10.1021/ja048022z
11. Chen B, Luo Y, Liang H, Xu J, Guo F, Zhang Y et al (2007) Optical properties of a tetradentate bis(β-diketonate) europium (III) complex. Spectrochim. Acta [A], doi:10.1016/j.saa.2007.10.041
12. Liang H, Chen B, Guo F, Guan J, Zhang Q, Li Z (2005) Luminescent polymer containing Eu chelates with different neutral ligands. Phys Status Solidi B 242:1087–1092, doi:10.1002/pssb.200402128
13. Gordon J, Ballato J, Jin J, Smith DW (2006) Spectroscopic properties as a function of fluorine content in Eu^{3+}: PMMA. J Polym Sci Pol Phys 44:1592–1596, doi:10.1002/polb.20818
14. Lee CI, Lim JS, Kim SH, Suh DH (2006) Synthesis and luminescent properties of a novel Eu-containing nanoparticle. Polymer (Guildf.) 47:5253–5258, doi:10.1016/j.polymer.2006.05.054
15. Yao XJ, Wang YW, Zhang XY, Zhang RS, Liu MC, Hu ZD et al (2002) Radial basis function neural network-based QSPR for the prediction of critical temperature. Chemometr Intell Lab 62:217–225, doi:10.1016/S0169-7439(02)00017-5
16. Xu J, Zheng Z, Chen B, Zhang Q (2006) A linear QSPR model for prediction of maximum absorption wavelength of second-order NLO chromophores. QSAR Comb Sci 25:372–379, doi:10.1002/qsar.200530143
17. Fitch WL, McGregor M, Katritzky AR, Lomaka A, Petrukhin R, Karelson M (2002) Prediction of ultraviolet spectral absorbance using quantitative structure-property relationships. J Chem Inf Comput Sci 42:830–840, doi:10.1021/ci010116u
18. Shi J, Luan F, Zhang H, Liu M, Guo Q, Hua Z et al (2006) QSPR study of fluorescence wavelengths ($\lambda_{ex}/\lambda_{em}$) based on the heuristic method and radial basis function neural networks. QSAR Comb Sci 25:147–155, doi:10.1002/qsar.200510142
19. Nantasenamat C, Isarankura-Na-Ayudhya C, Tansila N, Naenna T, Prachayasittikul V (2007) Prediction of GFP spectral properties using artificial neural network. J Comput Chem 28:1275–1289, doi:10.1002/jcc.20656
20. Li M, Ni N, Wang B, Zhang Y (2008) Modeling the excitation wavelengths (λ_{ex}) of boronic acids. J Mol Model 14:441–449, doi:10.1007/s00894-008-0293-0
21. Melby L, Rose N, Abramson E, Caris JC (1964) Synthesis and Fluorescence of Some Trivalent Lanthanide Complexes. J Am Chem Soc 86:5117–5125, doi:10.1021/ja01077a015
22. Stucchi EB, Scapari SL, Coutodossantos MA, Leite SRA (1988) Preparation, characterization and spectroscopy of the europium diphenylphosphinate complex. J Alloy Comp 275:89–92, doi:10.1016/S0925-8388(98)00280-1
23. Nageno Y, Takebe H, Morinaga K, Izumitani T (1994) Effect of modifier ions on fluorescence and absorption of Eu^{3+} in alkali and alkaline earth silicate glasses. J Non-Cryst Solids 169:228–294, doi:10.1016/0022-3093(94)90324-7
24. Hypercube (2000) HYPERCHEM. Hypercube, Gainesville
25. TALETE srl (2006) DRAGON for Windows (Software for Molecular Descriptor Calculations). TALETE, Milan
26. Liu H, Gramatica P (2007) QSAR study of selective ligands for the thyroid hormone receptor β. Bioorg Med Chem 15:5251–5261, doi:10.1016/j.bmc.2007.05.016
27. Holder AJ, Yourtee DM, White DA, Glaros AG, Smith R (2003) Chain melting temperature estimation for phosphatidyl cholines by quantum mechanically derived quantitative structure property

relationships. J Comput Aided Mol Des 17:223–230, doi:10.1023/A:1025382226037
28. Wessel MD, Jurs PC (1994) Prediction of reduced ion mobility constants from structural information using multiple linear regression analysis and computational neural networks. Anal Chem 66:2480–2487, doi:10.1021/ac00087a012
29. Hemmer MC, Steinhauer V, Gasteiger J (1999) Deriving the 3D structure of organic molecules from their infrared spectra. Vib Spectrosc 19:151–164, doi:10.1016/S0924-2031(99)00014-4
30. Jansson PA (1991) Neural networks: an overview. Anal Chem 63:357A–362A, doi:10.1021/ac00004a011
31. Xu L, Ball JW, Dixon SL, Jurs PC (1994) Quantitative structure-activity relationships for toxicity of phenols using regression analysis and computational neural networks. Environ Toxicol Chem 13:941–851, doi:10.1897/1552-8618(1994)13[841:QSRFTO]2.0.CO;2
32. Qi Y, Zhang Q, Xu L (2002) Correlation analysis of the structures and stability constants of gadolinium(III) complexes. J Chem Inf Comput Sci 42:1471–1475, doi:10.1021/ci020027x